ORIGINAL PAPER

Optimization of process parameters for autogenous TIG welding of austenitic stainless-steel SS-304

Anand Baghel[1] · Chaitanya Sharma[2] · Vikas Upadhyay[3] · Rajat singh[1]

Abstract

This work presents the effect of process parameters viz., current, speed, gas flow rate, and arc gap on characteristics of austenitic stainless steel SS304 bead-on plate welds and determines the optimal combination of parameters. Experiments were conducted as per Taguchi L9 orthogonal array and the effect of process parameters on weld bead profile, penetration depth, bead width, microstructure, and hardness were analysed. An optimum value was obtained for each process parameter to maximize penetration depth and hardness and minimize the bead width and HAZ. It was found that heat input per unit weld length is crucial in controlling the weld characteristics. Stronger inward flow patterns were responsible for beads with a narrower width and deeper penetration because of higher heat input however, excessive heat input was detrimental and produced wider beads and HAZ. Current and speed were most dominant in deciding weld characteristics than gas flow rate and arc gap. Predicted results are in close agreement with the confirmation experiments.

Keywords Austenitic stainless steel · Welding · Optimization · Bead profile · Microstructure · Hardness

1 Introduction

Austenitic stainless steel of 300 series were developed in early twentieth century in Germany and widely used in a variety of industrial applications. Addition of austenite stabilizing element like nickel, manganese and nitrogen develops austenite, a face cubic crystalline structure from ferrite. Also, specific composition, heat treatment and cooling rate are needed for its formation [1]. These nonmagnetic, work hardenable austenitic steels are widely used for diversified applications in automotive, aerospace, chemical, food, dairy, medical, home and architectural industries owing to their formability, ductility, toughness, weldability, corrosion and creep resistance [2, 3]. In general, applications of stainless steels in diversified areas requires joining of standard structural shapes by one or other welding techniques [4]. SS304 is weldable not only by arc welding techniques but also by new techniques like friction stir welding, cold metal transfer welding, etc. Friction stir welding is capable to produce high quality consistent, light similar and dissimilar welds with superior microstructure, mechanical, fatigue and corrosion behavior [5–7].

Tungsten inert gas (TIG) welding utilizes non-consumable tungsten electrode to produce arc for melting and joining of metals. TIG utilizes low-cost equipment and can produce high quality welds with an inert shielding gas like argon, helium, or a mixture to prevent air metal reactions. Though, TIG offers many advantages but low penetration depth (maximum of 3.5 mm in a single pass) renders it less appropriate for welding of thick plates [8]. Joining of thick plates (thickness greater than 3.5 mm) using the TIG welding necessitates preparation of a suitable groove geometry, multiple-pass welding, and filler material [9–14]. Multi-pass welding overcomes the limitation of low penetration depth of single pass TIG and was off late used for joining thick sections. However, it results in reduced productivity and increased welding costs on account of expenses on edge preparation, increased cost of filler metals, shielding gas and labor cost.

Other techniques to improve penetration during TIG welding include optimization of process parameters and use of

✉ Chaitanya Sharma
chaitanya.sharmaji@gmail.com

1 Department of Automobile Engineering, RJIT Tekanpur Madhya Pradesh, Gwalior, India

2 Department of Mechanical Engineering, BIT Sindri, Dhanbad, India

3 Mechanical Engineering Department, National Institute of Technology Patna, Patna, India

oxide, fluoride, and chloride-based fluxes, known as activated fluxes. In most cases, oxide-based fluxes offer deepest penetration, improved microstructural, and mechanical properties. Type of activated fluxes used varies from metal to metal, for example, SiO_2, TiO_2, Al_2O_3, and MnO_2 fluxes are preferred for joining of austenitic, duplex, and martensitic stainless steels [15–17]. The use of activated fluxes along with optimized parameters can enhance the penetration depth to greatest achievable level.

Optimization of processes parameters is crucial for the success of any welding process as it affects the quality and properties of weldments. Welding current, speed, gas flow rate, and arc gap are some of the process parameters which had most significant consequences on the heat input however, they affect weld heat input differently so as weld morphology and quality [6, 18–21]. In general, an increase in welding current, increases the melting rate of base metal due to increased heat input which in turn results in a greater weld pool size, thus increased bead dimensions [22–24]. Similar effect was also observed on decreasing the welding speed i.e., increased penetration depth since weld arc spends more time at a location and raises the temperature. Decrease in welding speed from 71.94 to 60.58 mm/min and increase in current from 100 to 300 A, increased the depth of penetration from 6.3 mm to 6.7 mm during welding of 10 mm thick P-22 grade steel [25]. Arc gap also affects the weld penetration. If the arc gap is too small, there is greater chances of tungsten contamination and leads to inconsistent weld penetration which causes shallow weld [26]. On the other hand, too large arc gap causes unstable and erratic welding arc which causes inconsistent weld penetration. It causes deep and narrow weld, which does not provide sufficient strength to weld [27, 28]. Welding speed and current were found the most influencing process parameter for controlling the hardness of HAZ and tensile strength of TIG dissimilar welds of AA6061-AA5083 aluminum alloy while use of non-optimal process parameters resulted in larger HAZ, porosity, voids, and other defects in larger numbers [20]. Greater gas flow prevents the molten metal from adverse outcomes of atmospheric gases and increase penetration. On increasing gas flow from 1 to 18 l/min, weld width increased from 5.42 mm to 9.12 mm because of higher rate of heat diffusion [29, 30]. Experiments were planned as per Taguchi L9 orthogonal array for welding 4.84 mm thick SS304. Optimal parameters (110 A current, 82 mm/min speed, and 13 l/min flow rate) produces superior HAZ hardness of 194 Hv possibly due to more ferrite content owing to rapid cooling rate at low heat input. High heat input resulted in lower hardness because slow cooling transformed the majority of ferrite into low hardness austenite [31].

In view of the literature review the present work aims to optimize the process parameters viz. welding current, speed, gas flow rate and arc gap using Taguchi L9 orthogonal array and investigate their influence on weld morphology, microstructure, and hardness using analysis of variance (ANOVA).

2 Experimental procedure

SS304 plates of dimension 100 mm $\times$ 30 mm $\times$ 6 mm were used as base metal. TIG, bead on plate welding was used in the experimental work. The nominal composition of base metal is given in Table 1 [32].

After being hand-ground to eliminate impurities like grease and dirt, the plates' surfaces were thoroughly cleaned using acetone. Bead-on-plate welding was completed using an air-cooled TIG welding machine having direct current electrode negative (DCEN) polarity (Electra-250, India). Thoriated tungsten and argon were used as electrodes and shielding gases for welding. The initial parameters for pilot experiment were selected based on literature review [31, 33, 34]. During pilot experiment, a current range between 80 and 120 A produced good welding; current below 80A did not cause penetration while current above 120 A melted the 6 mm thick plate. A feed setup was designed and fabricated to maintain the arc gap constant and the welding speed uniform, as shown in Fig. 1. The plates to be welded were placed over the welding platform, and the setup was then adjusted for the required welding speed and arc gap. Based on machine constraints and pilot experiments, the range and levels of input parameters and fixed parameter values were finalized, as shown in Table 2.

The Taguchi technique was utilized to reduce the number of experimental trials with selected levels of factors. A 3-level 4-factor design was selected to create a L-9 (3^4) orthogonal array from available Taguchi Designs. The signal to noise (S/N) ratio for each level is based on the S/N analysis. Larger-the-better criterion was considered for penetration depth, bead hardness and HAZ hardness, whereas smaller-the-better criterion was selected for bead width and HAZ width. The standard S/N formula for computing the type of response is mentioned in Eqs. (1) and (2).

$$\text{Larger the Better :} \ (S/N)_i = -10 \log\left[1/n \sum\nolimits_{j=1}^{2} 1/Y_{ij}^2\right] \quad (1)$$

$$\text{Smaller the Better :} \ (S/N)_i = -10 \log\left[1/n \sum\nolimits_{j=1}^{n} Y_{ij}^2\right] \quad (2)$$

where 'i' denotes the trial's number, 'Y_{ij}' denotes the quality of the ith trial and jth experiment, and 'n' denotes the total number of experiments [35].

The L9 orthogonal array is given in Table 3. The design is orthogonal, which means it can estimate the independent relationship between different response parameters and process parameters.

Table 1 Chemical composition of base metal SS304 (wt%)

Steel	Cr	Ni	C	Mn	Si	P	S	N
SS304	18–20	8–10.5	0.08	2	0.75	0.045	0.03	0.1

Fig. 1 Experimental setup for TIG welding **a** Chain sprocket and screw attachment for constant feed **b** vertical screw attachment used to control arc gap

(a)　(b)

Table 2 Details of welding parameters and weld condition

Current	Welding speed	Gas flow rate	Arc gap	Power source
85–95–105 A	1–2.5–3.5 mm/s	5–9–-3 l/min	1–2–3 mm	DCEN
Shielding gas	Electrode included angle	Electrode diameter	Material	Voltage
Argon	60	3 mm	SS304	20 V

Table 3 L9 orthogonal array with corresponding responses

Run	Control factors				Responses					
	Current (A)	Welding speed (mm/s)	Gas flow rate (l/min)	Arc gap (mm)	Penetration depth (mm)	Bead width (mm)	Aspect ratio (D/W)	HAZ width (mm)	Bead hardness (HV)	HAZ hardness (HV)
1	85	1	5	1	3.10	5.18	0.60	3.39	204.12	209.80
2	85	2.5	9	2	1.85	4.62	0.40	2.35	230.40	236.96
3	85	3.5	13	3	1.75	4.46	0.39	2.20	237.60	244.20
4	95	1	9	3	3.43	6.34	0.54	4.35	206.88	212.00
5	95	2.5	13	1	2.18	4.94	0.44	3.17	225.20	240.00
6	95	3.5	5	2	2.05	5.24	0.39	3.63	230.60	242.00
7	105	1	13	2	3.45	7.32	0.47	4.41	191.52	192.52
8	105	2.5	5	3	2.75	6.48	0.42	3.83	206.40	209.40
9	105	3.5	9	1	2.73	5.76	0.47	4.21	203.06	218.40

Bead-on-plate welding was performed using different *levels* of independent control factors as per Table 3. *A total of nine* bead-on-plate welds were made. After welding, specimen of *size* $20 \times 10 \times 6$ mm^3 were cut perpendicular to the weld bead with fusion zone at the centre. The samples for microscopy, hardness measurement, and confirmation tests were then cold-mounted using resin and hardener, which facilitates their polishing with ease. The mounted samples were then polished on a dual disk polisher (BAINPOL PMV, Chennai Metco India) using various grades of emery papers (120 μ to 2000 μ). Samples were first grounded using 120 μ SiC paper and then rotated by 90^0 for each higher grade of SiC paper. During polishing, a jet of water was used to cool the specimen and flush the debris away from the specimen. Finally, samples were polished on blazer and velvet cloth with alumina powder of 1 μ size. Polished samples were etched with an etchant comprising 2 g CuSO$_4$, 5 ml H$_2$SO$_4$, 10 ml HCl, and 10 ml H$_2$O to reveal the fusion zone, HAZ, and grain structure. The microstructure of weld beads was analyzed by optical microscope (DM750 M, Leica). Hardness was measured on polished and etched samples per ASTM E92-82 using a Vickers hardness tester (VM-50, SSS Instruments, India).
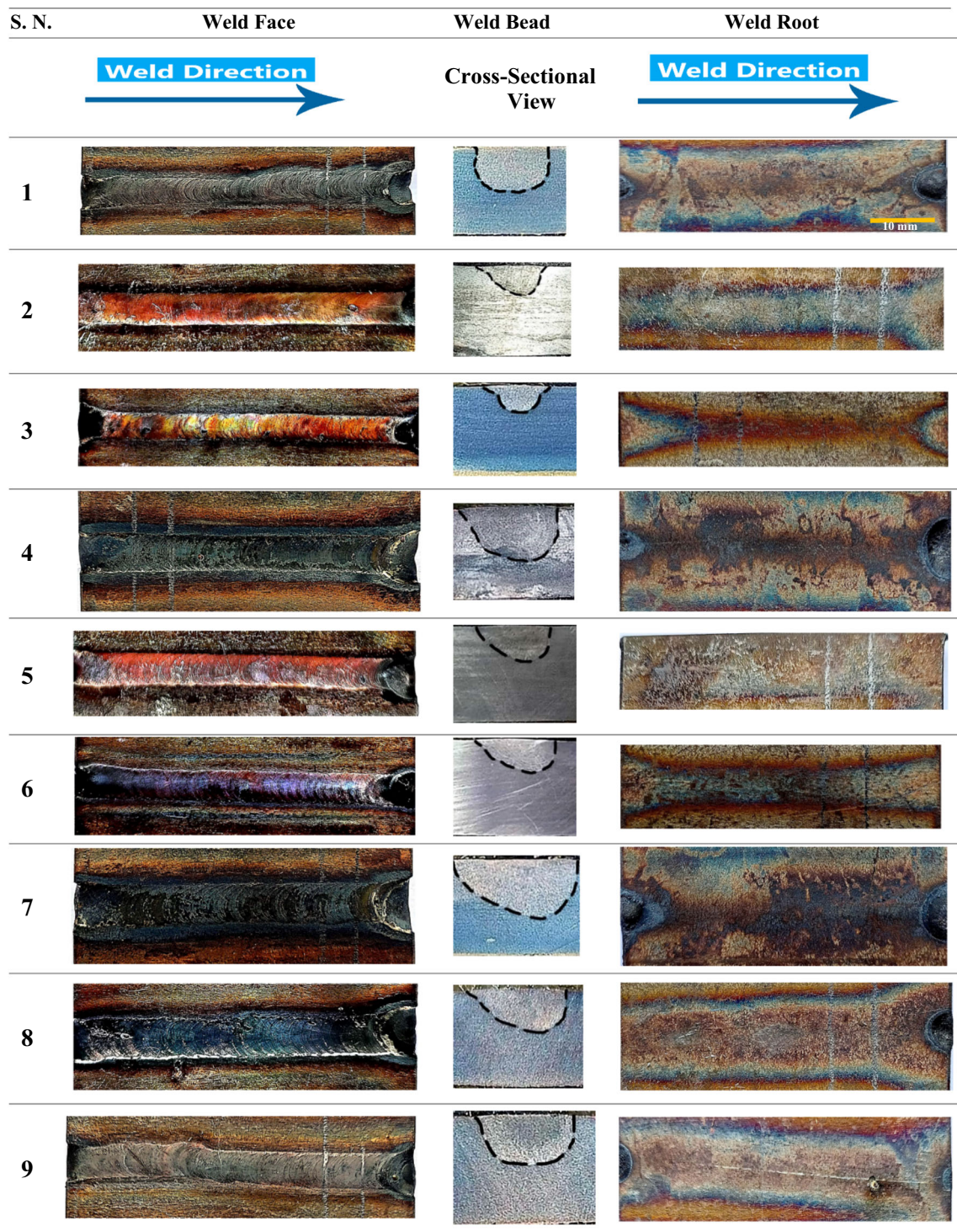
S. N.	Weld Face	Weld Bead	Weld Root
	Weld Direction →	Cross-Sectional View	Weld Direction →
1			
2			
3			
4			
5			
6			
7			
8			
9			

Fig. 2 Variation of weld morphology (Weld face, root, and profile) with welding parameters

3 Result and discussion

3.1 Weld morphology

The morphology of the bead on plate welds is presented in Fig. 2. The serial number is same as Taguchi L9 design presented in Table 3. The process parameters largely affect the appearance of the weld face, root, and bead as evident from Fig. 2 which is obvious because of varying heat input to welds.

A careful inspection of the deposited beads revealed that all the beads were free from visible weld defects. Beads were uniform, but their width was found to vary with welding parameters. Ripples were also visible on weld beads. A region with changed color was seen on the weld bead's root side. In general, the width of the region was found in direct relation to that of bead width at the crown. The wider crown of the bead had a wider root also. The shape of the bead varied with the change in parameters. It was symmetrical for experiment runs 1, 3, and 9, while the rest had an unsymmetrical profile. Trial run 7 was found to have the greatest penetration depth, followed by run 4 and 1. Run 3 of the experiment produced the lowest penetration depth, followed by run 2. The variation in penetration depth and bead profile can be attributed to changes in heat input per unit weld length due to change in parameters.

3.2 Microstructure

The base metal, HAZ, weld bead, fusion boundary, and partial fusion zone are visible in the microstructure images of the specimens. Figure 3 shows the microstructure images of the weld specimens fabricated as per the Taguchi design. Weld beads were defect-free, i.e., no evidence of defects, such as solidification cracking and porosity, was found during microstructure analysis. The base metal mostly consists of an austenitic phase. The HAZ comprises an austenite phase with large grain size. The grain size is larger near the weld bead and tends to decrease as it moves away from the weld center. During welding, weld metal cools rapidly because it is surrounded by partially melted fusion zone and HAZ, which have a temperature lower than molten weld pool. It creates a large temperature gradient causing faster weld metal cooling. The transformation of delta ferrite to austenite is incomplete, and more delta ferrite is retained in the weld metal after solidification.

Different weld zones have varying microstructures, as evident from the micrographs in Fig. 3. The central region of the weld bead exhibited a dendritic microstructure. Dendrite structure is found in the weld bead aligned along the cooling direction. The dendritic structure at the weld periphery has a longer dendritic arm of 85 μm and a smaller dendritic arm of 11 μm. These large and small dendrite arms were almost indistinguishable in the central fusion zone of the bead. HAZ size was found to vary from crown to root of the bead. The width of HAZ was found to be more near the weld face and smaller at the weld root hence widening it. The grain size of HAZ in the vicinity of the weld bead was 110 μm, and it gradually decreased to 45 μm on approaching the base metal. HAZ and base metal displayed the austenitic grain structure but were significantly coarsened. The degree of coarsening varied with the process parameters.

4 Statistical analysis

Statistical analysis was carried out to assess the impact of process input variables (current, speed, gas flow rate, and arc gap) on responses. Since some input factors had small contributions, these were pooled and studied using response tables of mean and a pooled analysis of variance. The delta value depicts the influence of a factor on response. The higher the delta value, the greater the rank, i.e., the influence of a factor on a response. Degree of freedom (DF), sequential sums of squares (Seq SS), adjusted sum of squares (Adj SS), adjusted mean squares (Adj MS), contribution (P), and contribution percentage (cont. %) were determined for all responses. The ratio of the mean square value of the model to the mean square value of the residual yields the model's F value. The significance of the parameters was determined with the help of the P-value. If the P-value is less than 0.05, the input parameter is statistically significant at a 95% confidence level. Otherwise, the term is insignificant and may be removed from the analysis. The R^2 score indicates how much of the variability in the data is explained by the ANOVA model. [24, 25].

4.1 Penetration depth

Penetration depth had to be maximized, so larger the better criterion is used for analysis. The response table for means of penetration depth is presented in Table 4. Welding speed had much higher delta values than current, while gas flow rate and arc gap exhibit approximately similar lowest delta values to vary their rank, i.e., influence. It can be concluded from the response table for means that the welding speed has the largest effect on penetration depth, followed by current, arc gap, and gas flow rate.

The variation of mean penetration depth with various input factors is shown by main effect plots for penetration depth, as shown in Fig. 4. Penetration depth varies differently with each input parameter. The mean value for penetration depth increased with current and decreased with welding speed. For the gas flow rate mean of penetration depth first increased to maximum and then decreased with further increase in gas flow rate. Arc gap has an opposite trend of variation of mean

Fig. 3 Evolution of microstructure in HAZs and fusion zone of weld beads with process parameters
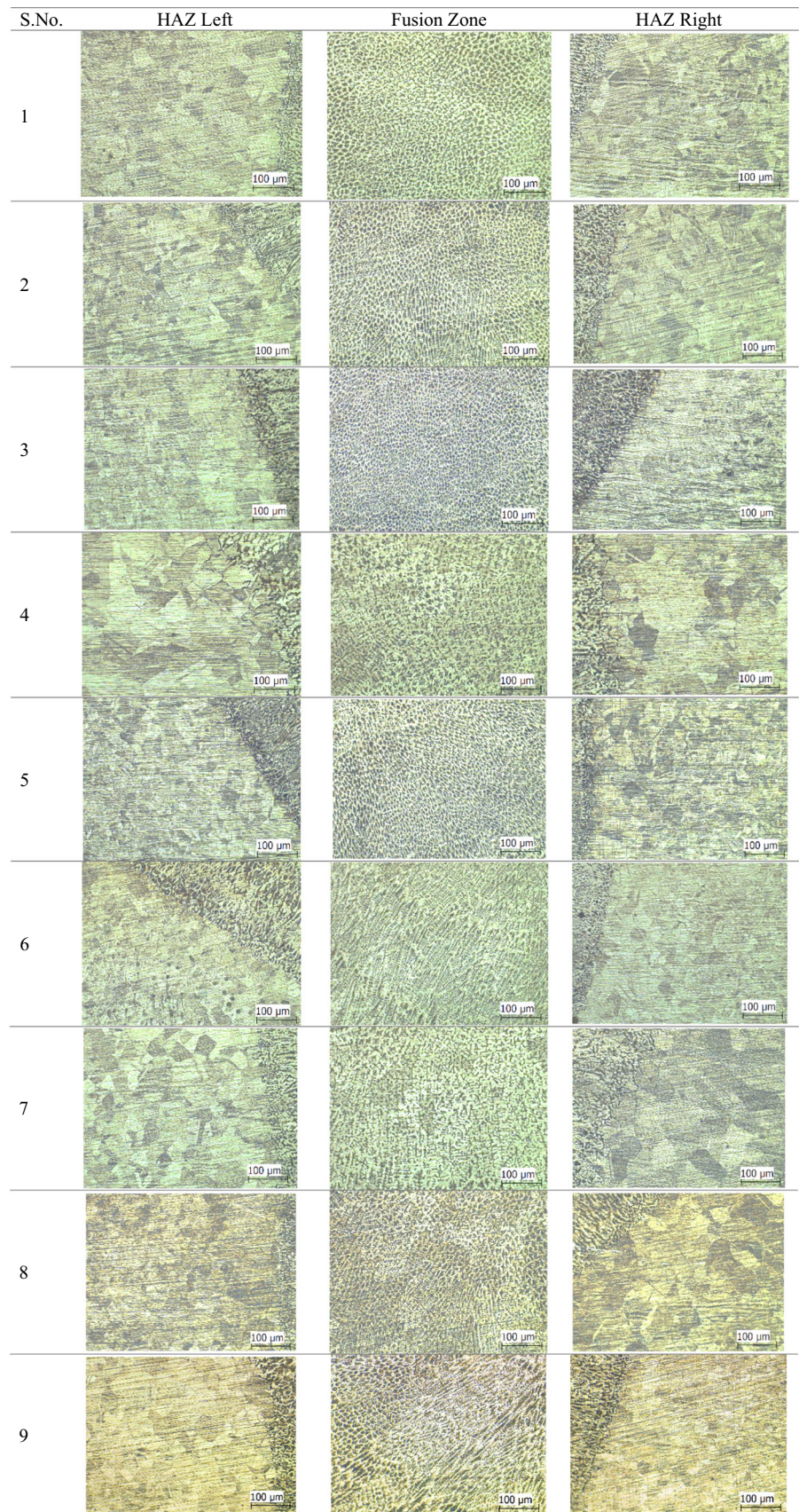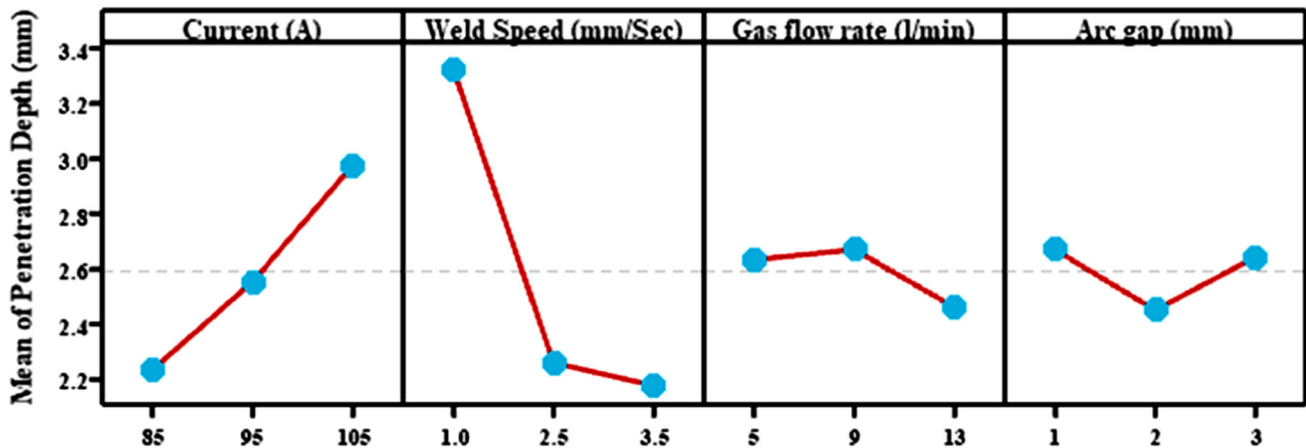
Table 4 Response table for means of penetration depth

Level	Current (A)	Welding speed (mm/s)	Gas flow rate (l/min)	Arc gap (mm)
1	2.233	3.327	2.633	2.670
2	2.553	2.260	2.670	2.450
3	2.977	2.177	2.460	2.643
Delta	0.743	1.150	0.210	0.220
Rank	2	1	4	3

Fig. 4 Main effect plot of means for penetration depth

to that of gas flow rate. The optimum maximum penetration depth recommended by main effect plots for means is obtained at 105 A current, 1 mm/s welding speed, 9 l/min gas flow rate, and 1 mm arc gap.

Table 5 summarizes the pooled variance of analysis for means of penetration depth. P-values less than 0.05 indicate model terms are significant. In this case, welding speed and current were significant model terms. Welding Speed had the highest (71.3%) contribution percentage followed by current (24.1%); therefore, both were statistically significant, whereas other factors, viz. arc gap and gas flow rate, were insignificant due to much less percentage contribution and hence pooled during analysis.

Heat generation by an electric arc is directly proportional to welding current and voltage. The ratio of the product of welding current (I) and voltage (E) divided by welding speed (V) is the amount of heat input per unit weld length (EI/V) and influences the cooling rate. Increased current at constant speed increases the heat input per unit weld length and vice versa. Therefore, increase in penetration depth with increasing current or decreasing speed is due to the higher heat input to weld, melting the faying edges easily. Increasing EI/V decreases the cooling rate and vice versa. It can be achieved by either increasing the current or decreasing speed. Slower cooling facilitates this owing to the higher peak temperature for a longer duration in a narrow region. It also affects the weld pool's surface tension, which decreases with increasing

temperature. Weld pool centre has lower surface tension than the surrounding outer region owing to the higher temperature. Molten metal flows from the low surface tension region to the high surface tension region, i.e., weld center to the outer region. This outward flow widens the weld bead and makes it shallow, as in the case of low current or high speed for which the cooling rate is low. Arc gap or arc length governs the speed of electrons. Short is the arc gap, low is the speed of electrons resulting in less weld pool heating on account of less bombing effect of electrons which in turn produces shallow weld. This lower penetration is due to decreased efficiency of welding heat transfer arising from enlarged anode diameter on account of higher heat generation [36]. An increase in helium gas flow rates from 5 l/min to 9 l/min increased the penetration slightly due to enhanced compression effect, i.e., arc constriction. At a higher flow rate, a small amount of helium escapes into the air, so a large amount of gas around the arc enhances compression effect, causing more heat transfer to the weld; hence, the increased penetration depth is obvious. In summary, stronger inward flow patterns are responsible for beads with narrower width and deeper penetration due to higher heat input. Similar results were also reported in literature [37].

Table 5 A pooled analysis of variance for penetration depth

Source	DF	Seq SS	Adj SS	Adj MS	F	P	Cont.% (%)
Current (A)	2	0.83416	0.83416	0.41708	10.30	0.026	24.1
Welding speed (mm/s)	2	2.46722	2.46722	1.23361	30.46	0.04	71.3
Gas flow rate (l/min) *	2	0.07549	–	–	–	–	–
Arc gap (mm)*	2	0.08649	–	–	–	–	–
Pooled error	4	0.16198	0.16198	0.04049			
Total	8	3.46336					

*Pooled factor

Table 6 Response table for means of bead width

Level	Current (A)	Welding speed (mm)	Gas flow rate (l/min)	Arc gap (mm)
1	4.753	6.280	5.633	5.293
2	5.507	5.347	5.573	5.727
3	6.520	5.153	5.573	5.760
Delta	1.767	1.127	0.060	0.467
Rank	1	2	4	3

4.2 Bead width

Bead width was minimized as per smaller the better criteria. The response table for means of bead width is presented in Table 6. Current has the greatest delta values followed by speed, arc gap, and gas flow rate, and rank also varied accordingly, so as their influence. It is evident from the response table of mean that current had the largest effect on the bead width while gas flow rate exhibited the least influence.

Figure 5 shows the main effect plot for mean of bead depth. The variation of bead width was like that of penetration depth with current and speed. However, the trend of variation of the mean of bead width with gas flow rate and arc gap was reversed to that of penetration depth, i.e., it first decreased with an increase in gas flow rate and remained constant after that. Bead width increased with arc gap for all values. Higher heat input forms a larger melt pool, so a wider weld bead. It is the reason for the increase in bead width with an increase in current and arc gap, and decrease in speed. Similar results were also reported by other researchers [38].

The optimum parameters for minimum bead width were current 85 A, weld speed 3.5 mm/s, gas flow rate 13 l/mm, and arc gap 1 mm, respectively.

Bead width must be kept to a minimum; hence smaller the better criterion was used for analysis. Table 7 summarizes the pooled analysis of variance for means of bead width. Welding current has the highest (64.5%) percentage contribution, followed by speed (29.8%), and is statistically significant. The contribution of the arc gap was only 5.6% of the total variation and is significantly smaller compared to current and speed however it has a value greater than 5% hence included in analysis despite a small contribution.

4.3 HAZ width

Smaller the better criterion was used for maximizing HAZ width. The response table for means of HAZ width is presented in Table 8. It may be concluded from the delta values of the response that the current has the largest effect on the HAZ width, followed by welding speed, gas flow rate and arc gap respectively.

The main effect plot for mean of HAZ width are presented in Fig. 6. Mean of HAZ width increased with an increase in current and had a similar trend to penetration depth and bead width. An increase in weld speed drops the mean of HAZ, but a further increase enhances the same. The trend is found like the variation of penetration depth with arc gap. With gas flow rate, mean of HAZ width first increased to maximum then decreased with further increase in gas flow rate. The same was found to decrease with the arc gap for all values. Like bead width, HAZ width is also found to rise with increasing heat input. A higher gas flow rate means more cooling, lower heat input, and narrow HAZ. The increase in arc gap does not seem to augment heat input to a level sufficient for enhancing HAZ width. The optimum values of various factors were current 85 A, speed 2.5 mm/s, gas flow rate 13 l/mm, and arc gap 2 mm, as suggested by main effect plot of means shown in Fig. 6.

Speed, current, gas flow rate, and arc gap had percentage contributions in descending order, as evident from the table of a pooled analysis of variance presented in Table 9. In this case, current and weld speed are crucial model factors, with P values of 0.009 and 0.023, respectively. Current and speed have a statistically significant percentage contribution of 67.60% and 26.60%, respectively. Current exhibited the
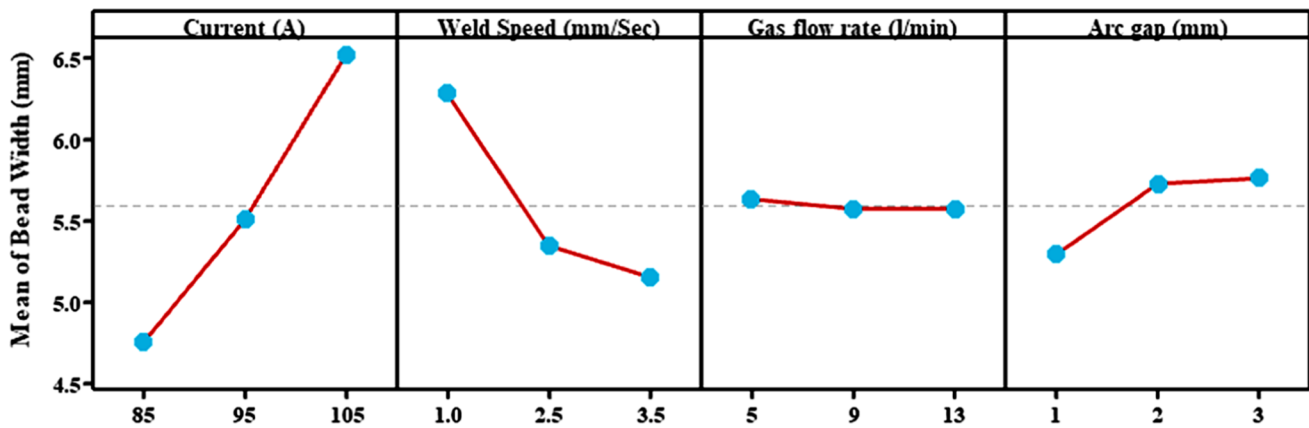
Fig. 5 Main effect plot of means for bead width

Table 7 A pooled analysis of variance for bead width

Source	DF	Seq SS	Adj SS	Adj MS	F	P	Cont.% (%)
Current	2	4.71547	4.71547	2.35773	654.93	0.002	64.5
Weld speed	2	2.17787	2.17787	1.08893	302.48	0.003	29.8
Gas flow rate*	2	0.0072					
Arc gap	2	0.4067	0.4067	0.20333	56.48	0.017	5.6
Pooled Error	2	0.0072	0.0072	0.0036			
Total	8	7.30720					

*Pooled factor

Table 8 Response table for means of HAZ width

Level	Current (A)	Welding speed (mm/s)	Gas flow rate (l/min)	Arc gap (mm)
1	2.647	4.050	3.617	3.590
2	3.717	3.117	3.637	3.463
3	4.150	3.347	3.260	3.460
Delta	1.503	0.933	0.377	0.130
Rank	1	2	3	4

highest percentage contribution, whereas the opposite is true for the arc gap. Current was the most significant factor, followed by speed and gas flow rate. On the other side, the arc gap had a small percentage contribution less than 5% and therefore it was pooled.

4.4 Bead hardness

Bead hardness was maximized as per larger the better criterion. The response table for the mean of bead hardness is presented in Table 10. Delta values were very high for current and welding speed compared to arc gap and gas flow rate. However, delta values were approximately the same for current and welding speed. It is evident from Table 10 that current dominates and is followed by welding speed, arc gap, and gas flow rate.

The main effect plots for the mean of bead hardness are presented in Fig. 7. Bead hardness declined with current. However, it augmented with speed for all other values. Bead hardness remained almost the same with the middle level of gas flow rate, beyond which it again augmented to the maximum value. Variation of bead hardness with arc gap had an opposite trend of variation to that of gas flow rate. Overall, the bead hardness mean varied in the opposite sense to that of penetration depth. The range of change in the mean of bead hardness was much more for current and speed than gas flow rate and arc gap, which had a relatively narrow range.

Heat input per unit weld length is the main factor governing the hardness distribution in the bead-on plate welds. It can be seen from Fig. 7 that hardness rapidly decreases with increasing heat input, i.e., with increasing current, decreasing speed, and gas flow rate. This is because the welding process's peak temperature and cooling rate depend on heat
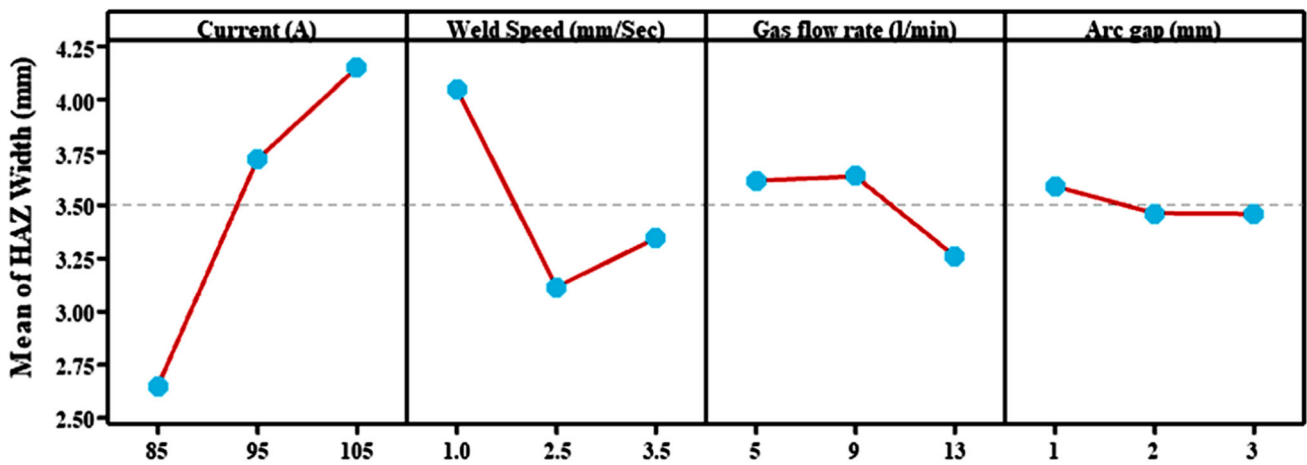
Fig. 6 Main effect plot for means of HAZ width

Table 9 A pooled analysis of variance for HAZ width

Source	DF	Seq SS	Adj SS	Adj MS	F	P	Cont.% (%)
Current (A)	2	3.59269	3.59269	1.79634	109.02	0.009	67.60
Weld speed (mm/s)	2	1.41869	1.41869	0.70934	43.05	0.023	26.60
Gas flow rate (l/min)	2	0.26949	0.26949	0.13474	8.18	0.109	5.07
Arc gap (mm)*	2*	0.03296					
Pooled error	2	0.03296	0.03296	0.01648			
Total	8	5.31382					

*Pooled factor

Table 10 Response table for the mean of bead hardness

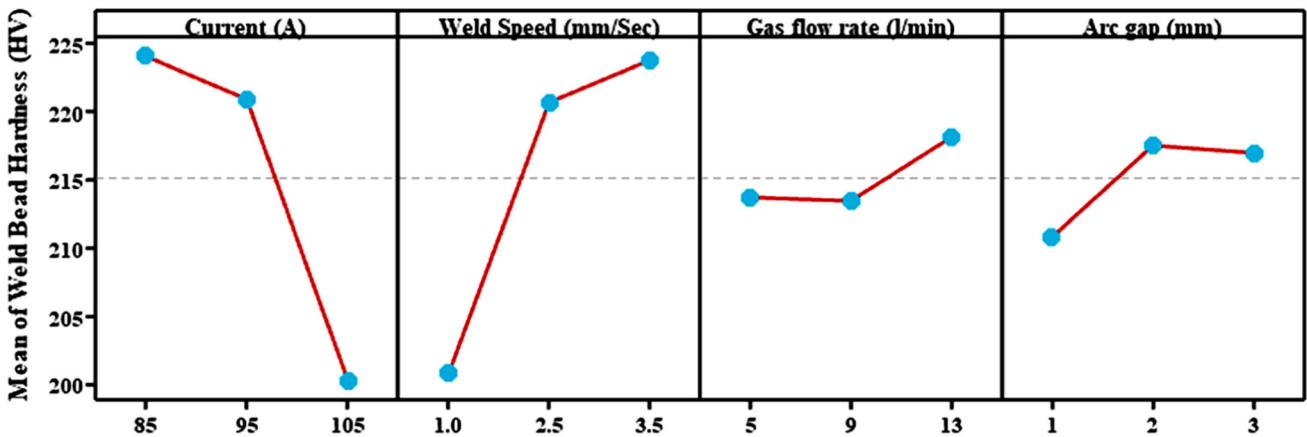| Level	Current (A)	Welding speed (mm/s)	Gas flow rate (l/min)	Arc gap (mm)
1	224.0	200.8	213.7	210.8
2	220.9	220.7	213.4	217.5
3	200.3	223.8	218.1	217.0
Delta	23.7	22.9	4.7	6.7
Rank	1	2	4	3

Fig. 7 Main effect plot for means of bead hardness

input and affect microstructure evolution greatly. Higher the heat input, lower is the cooling rate, which decreases the weld bead hardness because of coarsening and low volume of delta ferrite. Wichan et al. [25] and Bansod et al. reported similar results [39]. High speed for welding of low nickel austenitic stainless steel increases weld hardness. This was attributed to faster weld cooling owing to high speed, forming microstructure with finer grains and significant volumes of delta-ferrite. Increased gas flow rate beyond a medium level is believed to increase the cooling rate and hardness. Similarly, an increase in hardness with an increase in arc gap up to medium level is due to a faster cooling rate due to low heat input. A decrease in hardness with an increase in arc gap beyond the medium level may be due to a lower cooling rate owing to excessive heat input. The optimum values of process factors for maximum bead hardness were current 85 A, speed 3.5 mm/s, gas flow rate 13 l/min, and arc gap 2 mm, as evident from Fig. 7.

Current and speed have almost similar percentage contribution of 48.60% and 45.30%, respectively; thus, they were statistically significant, while other two factors, arc gap and gas flow rate, have a very low percentage contribution. Thus, arc gap and gas flow rate were pooled out, being the most insignificant factor, as seen from Table 11.

4.5 HAZ hardness

HAZ Hardness was maximized as per the larger the better criterion for analysis. Delta values were very high for speed and current compared to gas flow rate and arc gap. Speed exhibited the greatest delta value and arc gap least one. Speed had the most dominating effect on the mean of HAZ hardness than current, arc gap, and gas flow rate, as evident from the response table for means of HAZ hardness presented in Table 12.

The mean of HAZ hardness declined with current and arc gap; however, it increased with speed and gas flow rate for all the values used, as seen from the main effect plots of the mean of HAZ hardness presented in Fig. 8. The trend of variation was found like that of bead hardness. Further, the range of change in the mean of HAZ hardness was much wider for speed and current than gas flow rate and arc gap, which had a very narrow range. The variation of HAZ hardness with process parameters is like bead hardness. Higher the heat input lower the cooling rate, and greater the HAZ hardness. The decrease in HAZ hardness is due to grain coarsening because of the weld thermal cycle. This work's findings are consistent with those of Vashishtha et al. [40] and Somrerk et al. [41]

The optimum values of process factor for maximum HAZ hardness were; current 95A, speed 3.5 mm/s, gas flow rate 13 l/min, and arc gap 2 mm, respectively, recommended by main effect plots for mean of HAZ hardness presented in Fig. 8.

Speed and current both have very high contribution percentages of 42.53% and 55.76%, respectively; therefore, were statistically significant. Arc gap and gas flow rate were statistically insignificant; hence, they were pooled out as evident from the pooled analysis of variance for the mean of HAZ hardness presented in Table 13.

5 Summary of statistical analysis

It can be inferred from Tables 5, 7, 9, 11, and 13 that all the input parameters do not have a significant contribution so the results have been summarized and presented in Table 14, which enlists optimal values of input parameters that have a significant contribution on responses.

It is evident that current and welding speed are the most contributing parameters whereas arc gap and gas flow rate has almost insignificant contribution except for bead width and HAZ width respectively in the investigated range of parameters.

Regression models were developed for prediction of each of the response parameters with the help of the experimental data and are presented below.

$$\text{Penetration Depth} = 0.40 + 0.0372 \times \text{Current} - 0.480 \times \text{Welding Speed} - 0.0217 \times \text{Gas Flow Rate} - 0.013 \times \text{Arc Gap} \tag{3}$$

$$\text{Bead Width} = -2.11 + 0.0883 \times \text{Current} - 0.464 \times \text{Welding Speed} - 0.0075 \times \text{Gas Flow Rate} + 0.233 \times \text{Arc Gap} \tag{4}$$

$$\text{HAZ Width} = -2.39 + 0.0752 \times \text{Current} - 0.308 \times \text{Welding Speed} - 0.0446 \times \text{Gas Flow Rate} - 0.065 \times \text{Arc Gap} \tag{5}$$

$$\text{Bead Hardness} = 294 - 1.19 \times \text{Current} + 9.49 \times \text{Welding Speed} + 0.550 \times \text{Gas Flow Rate} + 3.08 \times \text{Arc Gap} \tag{6}$$

$$\text{HAZ Hardness} = 301 - 1.18 \times \text{Current} + 12.4 \times \text{Welding Speed} + 0.65 \times \text{Gas Flow Rate} - 0.43 \times \text{Arc Gap} \tag{7}$$

5.1 Confirmation experiments

The regression models were used to predict the value of the response parameters for optimal set of input parameters and experimental trials were also conducted for each set of optimal input parameters. The predicted and experimental values thus obtained are presented in Table 15. It is evident that predicted values were very close to experimental ones i.e., lies within $\pm$ 10% of actual ones. The squares marked with green shows those responses which are maximized whereas red ones show the minimized one.

Some numerical trials were carried out to determine the responses at the lowest, mid, and highest level of all the input parameters for better understanding of the process.
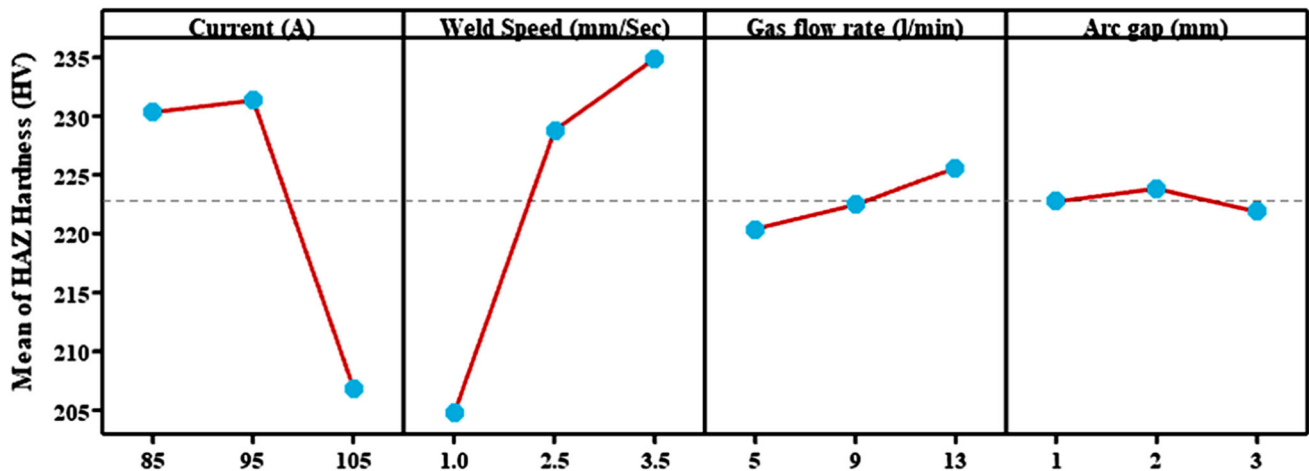
Table 11 Pooled analysis of variance for means of bead hardness

Source	DF	Seq SS	Adj SS	Adj MS	F	P	Cont.% (%)
Current (A)	2	995.21	995.211	497.606	15.98	0.012	48.60
Welding speed (mm/s)	2	927.65	927.645	463.823	14.90	0.014	45.30
Gas flow rate (l/min)*	2	41.14					
Arc gap (mm)*	2	83.40					
Pooled error	4	124.54	124.54	31.13			
Total	8	2047.40					

*Pooled factor

Table 12 Response table for means of HAZ hardness

Level	Current (A)	Welding speed (mm/s)	Gas flow rate (l/min)	Arc gap (mm)
1	230.3	204.8	220.4	222.7
2	231.3	228.8	222.5	223.8
3	206.8	234.9	225.6	221.9
Delta	24.6	30.1	5.2	2.0
Rank	2	1	3	4

Fig. 8 Main effect plot for means of HAZ hardness

Table 13 A pooled analysis of variance for means of HAZ hardness

Source	DF	Seq SS	Adj SS	Adj MS	F	P	Cont.% (%)
Current (A)	2	1158.67	1158.67	579.33	49.83	0.001	42.53
Welding speed (mm/s)	2	1519.22	1519.22	759.61	65.34	0.001	55.76
Gas flow rate (l/min) *	2	40.71					
Arc gap (mm)*	2	5.79					
Pooled Error	4	46.50	46.50	11.63			
Total	8	2724.38					

*Pooled factor

Table 14 Summary of significant factors for each response

Response	Current (A)	Welding speed (mm/s)	Gas flow rate (l/min)	Arc gap (mm)
Penetration depth (mm)	105	1	*	*
Bead width (mm)	85	3.5	*	1
HAZ width (mm)	85	2.5	13	*
Bead Hardness (HV)	85	3.5	*	*
HAZ hardness (HV)	95	3.5	*	*

*Parameters having insignificant contribution

Table 15 Comparison of predicted and experimental optimal parameters

Responses	Current (A)	Speed (mm/s)	Gas Flow Rate (l/min)	Arc Gap (mm)	Optimal Value		Percentage error in prediction	Predicted Values when all input parameters are at		
					Predicted	Experimental		Lowest Level	Mid Level	Highest Level
Penetration Depth (mm)	105	1	13	2	3.62	3.45	4.70	2.96	2.51	2.3
Bead Width(mm)	85	3.5	13	1	3.91	4.2	-7.42	5.13	5.52	6.14
HAZ width (mm)	85	2.5	13	2	2.52	2.28	9.52	3.41	3.45	3.65
Bead Hardness (HV)	85	3.5	13	2	239.38	237	0.99	208.17	215.79	218.66
HAZ Hardness (HV)	95	3.5	13	2	239.89	244	-1.71	215.92	224.89	227.66

The values thus obtained are presented in the last columns of the Table 15 and the highest or lowest value are marked as green or red among the three obtained values as per the response requirement. It is evident that the Taguchi technique has provided the optimal results with minimum number of experiments. The results were far better than the results in numerical trials.

6 Conclusions

The effect of input factors for tungsten inert gas welding such as current, speed, gas flow rate, and arc gap on penetration depth, bead width, HAZ width, bead hardness, and HAZ hardness were examined and optimized by using Taguchi orthogonal array and pooled analysis of variance. The selection of input factors and their level is vital for creating high-quality welds with superior characteristics. No solidification cracking was observed in the developed welds for a selected range of process parameters, while the same was seen during trial runs at 110 A current and a speed of 1 mm/s. Current and speed were the most dominating input factors. Heat input per unit weld length influences the weld characteristics profoundly because melt flow and cooling rate depend on it. An increase in current and arc gap increases the heat input whereas speed and gas flow rate minimize the same. Penetration depth is augmented with an increase in current and a decrease in speed. Regression models were developed for the response parameters and these models were compared with the values of the confirmation experiments. Predicted results are in excellent agreement with confirmation experiments. Taguchi technique has clearly helped to reduce the number of experiments, while analysis of variance has

helped in studying the influence of responses. In future, influence of process parameters and their interaction on tensile properties, fatigue and corrosion behaviour may be investigated. Use of activated fluxes to enhance weld penetration and mechanical properties may also be explored in detail.

References

1. Padilha, A.F., Rios, P.R.: Decomposition of austenite in austenitic stainless steels. ISIJ Int. **42**, 325–337 (2002)
2. Singh, A.K., Dey, V., Rai, R.N.: Techniques to improveweld penetration in TIG welding (A review). Mater. Today Proc. **4**, 1252–1259 (2017). https://doi.org/10.1016/j.matpr.2017.01.145
3. Singh, N.K.: Performance of activated TIG welding in 304 austenitic stainless steel welds. Mater. Today Proc. **4**, 9914–9918 (2017). https://doi.org/10.1016/j.matpr.2017.06.293
4. Padilha, A.F., Plaut, R.L., Rios, P.R.: Stainless steel heat treatment. Steel Heat Treat. Metall. Technol. (2006). https://doi.org/10.1081/e-eisa-120053057
5. Sharma, C., Upadhyay, V.: Microstructure and mechanical behavior of similar and dissimilar aa2024 and AA7039 friction stir welds. Eng. Rev. **41**, 21–33 (2020). https://doi.org/10.30765/ER.1533
6. Verma, V., Singh, A., Pandey, A.K., Sharma, C., Sonia, P., Saxena, K.K.: Experimental investigation of tensile properties and microstructure of TIG welded dissimilar joints of Al6061/Al5083 Aluminium alloy. Indian J. Eng. Mater. Sci. **29**, 262–270 (2022). https://doi.org/10.56042/ijems.v29i2.46110
7. Sharma, C., Dwivedi, D.K., Kumar, P.: Friction stir welding of Al-Zn- Mg alloy AA7039. In: Suarez, C.E. (ed.) Light Metals 2012, pp. 503–507. Springer, Cham (2016)
8. Kulkarni, A., Dwivedi, D.K., Vasudevan, M.: Effect of oxide fluxes on activated TIG welding of AISI 316L austenitic stainless steel. Mater. Today Proc. **18**, 4695–4702 (2019). https://doi.org/10.1016/j.matpr.2019.07.455
9. Durgutlu, A.: Experimental investigation of the effect of hydrogen in argon as a shielding gas on TIG welding of austenitic stainless steel. Mater. Design **25**(1), 19–23 (2004)
10. Wu, C.S., Gao, J.Q.: Analysis of the heat flux distribution at the anode of a TIG welding arc. Comput. Mater. Sci. **24**(3), 323–327 (2002)
11. Tseng, K.H., Chou, C.P.: The study of nitrogen in argon gas on the angular distortion of austenitic stainless steel weldments. J. Mater. Process. Technol. **142**, 139–144 (2003). https://doi.org/10.1016/S0924-0136(03)00593-4
12. Anders, A.: Tracking down the origin of arc plasma science-II. early continuous discharges. IEEE Trans. Plasma Sci. **31**, 1060–1069 (2003). https://doi.org/10.1109/TPS.2003.815477
13. Lu, S., Li, D., Fujii, H., Nogi, K.: Time dependant weld shape in Ar-O-2 shielded stationary GTA welding. (2007)
14. Lu, S., Fujii, H., Nogi, K.: Arc ignitability, bead protection and weld shape variations for He–Ar–O2 shielded GTA welding on SUS304 stainless steel. J. Mater. Process. Technol. **209**(3), 1231–1239 (2008). https://doi.org/10.1016/j.jmatprotec.2008.03.043
15. Huang, H.Y.: Effects of shielding gas composition and activating flux on GTAW weldments. Mater. Des. **30**, 2404–2409 (2009). https://doi.org/10.1016/j.matdes.2008.10.024
16. Huang, H.Y.: Argon-hydrogen shielding gas mixtures for activating flux-assisted gas tungsten arc welding. Metall. Mater. Trans. A Phys. Metall. Mater. Sci. **41**, 2829–2835 (2010). https://doi.org/10.1007/s11661-010-0361-9
17. Ghumman, K.Z., Ali, S., Din, E.U., Mubashar, A., Khan, N.B., Ahmed, S.W.: Experimental investigation of effect of welding parameters on surface roughness, micro-hardness and tensile strength of AISI 316L stainless steel welded joints using 308L filler material by TIG welding. J. Mater. Res. Technol. **21**, 220–236 (2022). https://doi.org/10.1016/j.jmrt.2022.09.016
18. Koli, Y., Aravindan, N.Y.S.: Enhancement of mechanical properties of 6061 / 6082 dissimilar aluminium alloys through ultrasonic - assisted cold metal transfer welding. Arab. J. Sci. Eng. (2021). https://doi.org/10.1007/s13369-021-05844-9
19. Prakash, A., Abebe, H., Seetharaman, S., Vijayakumar, S.: Materials Today: proceedings characterization and analysis of TIG welded stainless steel 304 alloy plates using radiography and destructive testing techniques. Mater. Today Proc. (2021). https://doi.org/10.1016/j.matpr.2021.06.305
20. Sharma, C., Upadhyay, V., Tripathi, A.: Effect of welding processes on tensile behavior of aluminum alloy joints. Int. J. Mech. Mech. Eng. **9**(12), 2051–2054 (2015)
21. Wang, J., Shi, Y., Cui, Y., Wang, Z.: Investigation of the relationship between voltage and arc length of K-TIG welding under penetrated condition. Int. J. Adv. Manuf. Technol. **120**, 3843–3857 (2022). https://doi.org/10.1007/S00170-022-09008-3
22. Huang, Y., Fan, D., Shao, F.: Alternative current flux zoned tungsten inert gas welding process for aluminium alloys. Sci. Technol. Weld. Joining **17**(2), 122–127 (2012). https://doi.org/10.1179/1362171811Y.0000000087
23. Kumar, S., Shahi, A.S.: Effect of heat input on the microstructure and mechanical properties of gas tungsten arc welded AISI 304 stainless steel joints. Mater. Design **32**(6), 3617–3623 (2011)
24. Bhavsar, A.N., Patel, V.A.: Influence of process parameters of TIG welding process on mechanical properties of SS304L welded joint. Int. Res. J. Eng. Technol. **3**(5), 977–981 (2016)
25. Pavan, A.R., Arivazhagan, B., Vasudevan, M.: Process Parameter optimization of a-TIG welding on P22 Steel. In: Lecture Notes in Mechanical Engineering. pp. 99–113. Springer (2020)
26. Baghel, A., Sharma, C., Rathee, S., Srivastava, M.: Activated flux TIG welding of dissimilar SS202 and SS304 alloys: effect of oxide and chloride fluxes on microstructure and mechanical properties of joints. Mater. Today Proc. **47**, 7189–7195 (2020). https://doi.org/10.1016/j.matpr.2021.07.199
27. Baghel, A., Sharma, C., Rathee, S., Srivastava, M.: Influence of activated flux on micro-structural and mechanical properties of AISI 1018 during MIG welding. Mater. Today Proc. **47**, 6947–6952 (2020). https://doi.org/10.1016/j.matpr.2021.05.210
28. Chakraborty, A., Sharma, C., Rathee, S., Srivastava, M.: Influence of activated flux on weld bead hardness of MIG welded austenitic stainless steel. Mater. Today Proc. **47**, 6884–6888 (2020). https://doi.org/10.1016/j.matpr.2021.05.168
29. Gadewar, S.P., Swaminadhan, P., Harkare, M.G., Gawande, S.H.: Experimental Investigations of Weld Characteristics for a Single Pass Tig Welding With Ss304. Int. J. Eng. Sci. Technol. **2**, 3676–3686 (2010)
30. Durgutlu, A.: Experimental investigation of the effect of hydrogen in argon as a shielding gas on TIG welding of austenitic stainless steel. Mater. Design **25**(1), 19–23 (2004). https://doi.org/10.1016/j.matdes.2003.07.004
31. Babbar, A., Kumar, A., Jain, V., Gupta, D.: Enhancement of activated tungsten inert gas (A-TIG) welding using multi-component TiO2-SiO2-Al2O3 hybrid flux. Meas. J. Int. Meas. Confed. (2019). https://doi.org/10.1016/j.measurement.2019.106912
32. Chemical composition of stainless steel, http://www.yamco-yamashin.com/en/products/guide_stainless_steel.html
33. Vasudevan, M.: Effect of A-TIG Welding process on the weld attributes of type 304LN and 316LN stainless steels. J. Mater. Eng. Perform. **26**, 1325–1336 (2017). https://doi.org/10.1007/s11665-017-2517-x
34. Liu, G.H., Liu, M.H., Yi, Y.Y., Zhang, Y.P., Luo, Z.Y., Xu, L.: Activated flux tungsten inert gas welding of 8 mm-thick AISI 304

austenitic stainless steel. J. Cent. South Univ. **22**, 800–805 (2015). https://doi.org/10.1007/s11771-015-2585-8

35. Huang, H.: Effects of activating flux on the welded joint characteristics in gas metal arc welding. Mater. Des. **31**, 2488–2495 (2010). https://doi.org/10.1016/j.matdes.2009.11.043
36. Patel, N.P., Vora, J.J., Badheka, V.J., Upadhyay, G.H.: Materials today: proceedings review on the use of activated flux in arc and beam welding processes. Mater. Today Proc. (2020). https://doi.org/10.1016/j.matpr.2020.07.218
37. Anawa, E.M., Olabi, A.G.: Using Taguchi method to optimize welding pool of dissimilar laser-welded components. Opt. Laser Technol. **40**, 379–388 (2008). https://doi.org/10.1016/j.optlastec.2007.07.001
38. Sivakumar, J., Nanda Naik, K.: Optimization of weldment in bead on plate welding of nickel based superalloy using Activated flux tungsten inert gas welding (A-TIG). Mater. Today Proc. **27**, 2718–2723 (2019). https://doi.org/10.1016/j.matpr.2019.11.327
39. Bansod, A.V., Patil, A.P., Moon, A.P., Shukla, S.: Microstructural and electrochemical evaluation of fusion welded low-nickel and 304 SS at different heat input. J. Mater. Eng. Perform. **26**, 5847–5863 (2017). https://doi.org/10.1007/s11665-017-3054-3
40. Vashishtha, H., Taiwade, R.V., Khatirkar, R.K., Ingle, A.V., Dayal, R.K.: Welding behaviour of low nickel chrome-manganese stainless steel. ISIJ Int. **54**, 1361–1367 (2014). https://doi.org/10.2355/isijinternational.54.1361
41. Chandra-Ambhorn, S., Saranyachot, P.: Effect of the H2 content in shielding gas on the microstructure and oxidation resistance of Fe$-$15.7 wt.% Cr$-$ 8.5 wt.% Mn steel GTA welds. J. Mater. Process. Technol. **268**, 18–24 (2019)